Electronic transport properties of capped-carbon-nanotube-based molecular junctions with multiple N and B dopants

ZHAO Peng[1]* & LIU DeSheng[2]

[1] School of Physics and Technology, University of Jinan, Jinan 250022, China;
[2] State Key Laboratory of Crystal Materials, School of Physics, Shandong University, Jinan 250100, China

By applying non-equilibrium Green's function in combination with density functional theory, we investigated the electronic transport properties of capped-carbon-nanotube-based molecular junctions with multiple N and B dopants. The results show that the electronic transport properties are strongly dependent on the numbers and positions of N and B dopants. Best rectifying behavior is observed in the case with one N and one B dopants, and it is deteriorated strongly with the increasing dopants. The rectifying direction is even reversed with the change of doping positions. Moreover, obvious negative differential resistance behavior at very low bias is observed in some doping cases.

carbon nanotube, rectifying, negative differential resistance, non-equilibrium Green function, density functional theory

Since its discovery in 1991 by Iijima, carbon nanotubes (CNTs) have shown to possess most remarkable electronic and mechanical properties [1]. Due to its high aspect ratio, a CNT can be considered as an one-dimensional quantum wire. Various applications in nanoscale devices have been proposed [2–6]. Along with the development of synthesizing technologies, doped single-wall carbon nanotubes (SWCNTs) have attracted more and more interest due to its potential applications in diodes and field-effect transistors [7,8]. Because they possess similar atomic radii to that of C, N and B atoms are the most commonly used dopants. Such doping has already been achieved by a variety of techniques, including arc discharge [9], pyrolysis [10], chemical vapor deposition [11], and substitution reactions [12]. Through the doping of N and B atoms, it is possible to provide more control of the electronic transport properties of a SWCNT [3,9]. Recently, we investigated the electronic transport properties of single-B-doped and single-N/B-doped capped-SWCNT junctions, and found obvious negative differential resistance (NDR) and rectifying behavior [13,14].
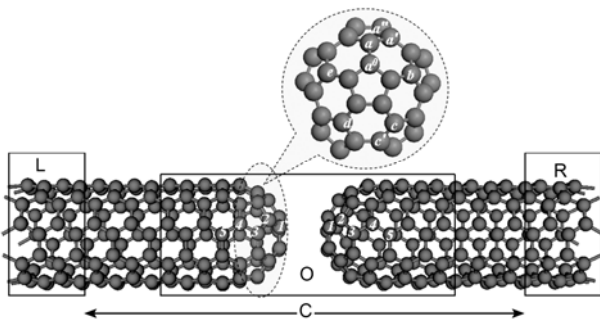
Though substantial progress has been made in chemical doping over the past decade, it is still very difficult to precisely control the doping concentration and doping positions. Fortunately, we can investigate these factors theoretically. In the present work, by applying non-equilibrium Green's function (NEGF) formalism in combination with density functional theory (DFT), we further investigated the effects of multiple N and B dopants on the electronic transport properties of the capped-SWCNT junctions.

Figure 1 shows the schematic of N/B-doped capped-SWCNT(5,5) junction. Both capped-SWCNT(5,5) electrodes are closed with fullerene hemispheres with opposing N and B atoms. The N atoms dope at the left part and the B atoms dope at the right part of the junction. Though there many doping positions, our investigations of electronic transport are concentrated on the doping in the second layer of the cap region, because we found in previous work that the best rectifying performance can be obtained when the N/B atom dopes at this layer [14]. Therefore, we have increased the number of N/B atoms at this layer in order to investigate
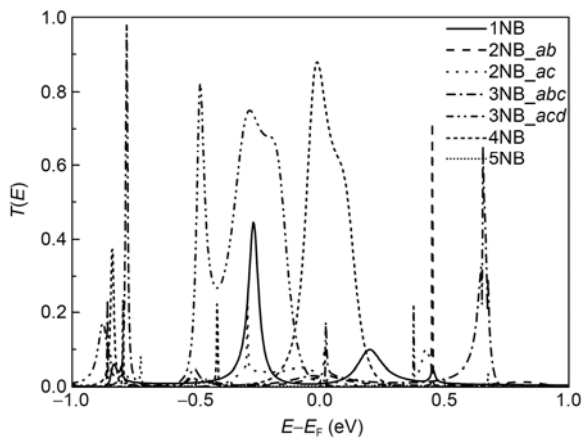
*Corresponding author (email: ss_zhaop@ujn.edu.cn)

how rectifying behavior responds to the number of N/B atoms and their doping positions. As shown in Figure 1, given the symmetry, we considered seven models: 1NB, 2NB_*ab*, 2NB_*ac*, 3NB_*abc*, 3NB_*acd*, 4NB and 5NB, where NB means N and B atoms, 1–5 mean the numbers of N and B atoms, and *a–c* mean possible doping positions in the second layer. In theoretical simulations, the molecular junction is divided into three regions: the left semi-infinite electrode (L), the central scattering region (C), and the right semi-infinite electrode (R). As stated in our previous work [13,14], the distance between the two tips is fixed at 0.35 nm and the structures comprising the O region have been optimized using the SIESTA package [15], and the electron transport calculations have been performed using the ATK package [16,17], which combines DFT and NEGF.

Figure 2 shows the transmission spectra under zero bias for seven models. It is clear that transmission spectra depend strongly on the number of doping atoms and doping positions. For 1NB junction, there are two transmission peaks around the Fermi level E_F. For 4NB junction, a broad and strong transmission peak right lies in E_F. For 3NB_*acd*

junction, there are two strong transmission peaks just below E_F. For other junctions, the transmission peaks are very weak around E_F.

Figure 3 shows the calculated *I-V* curves for seven models with the bias varying from −1.0 to 1.0 V. It is clear that *I-V* curves depend strongly on the number of doping atoms and doping positions. Obvious rectifying behavior is observed in 1NB junction since the forward-bias current $I_{forward}$ is significantly larger than the backward-bias one $I_{backward}$ in the whole range of the considered biases (which can be seen more clearly from the inset in Figure 3). When more doping atoms (except for 4NB case) are introduced into the carbonaceous lattice, the $I_{forward}$ is weakened, while the $I_{backward}$ is enhanced. As a result, the rectifying performance is deteriorated. As a figure of merit, the rectification ratios $R(V) = |I_{forward}(V)/I_{backward}(V)|$ versus bias V for seven models are plotted in Figure 4. One can see that the rectification ratio is
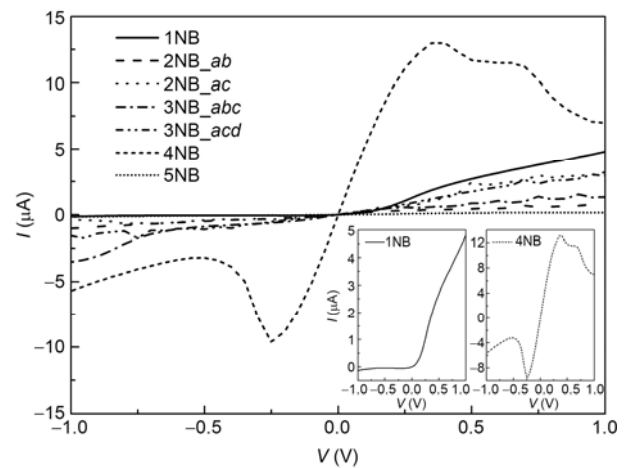

Figure 1 Schematic illustration of the capped-SWCNT junction showing dopant positions and division into regions for calculation purposes. The numbers 1–5 indicate the layers of carbon atoms while the characters a^0, *a–e*, *a'(c')*, *a''* indicate the doping positions in the first, second, third, and fourth layers, respectively.
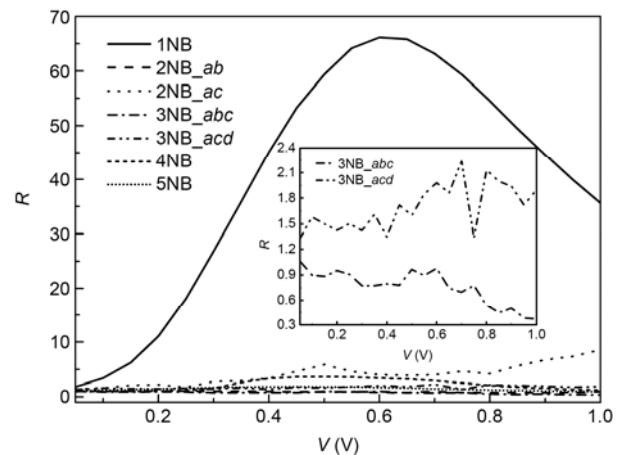

Figure 3 *I-V* curves for models 1NB, 2NB_*ab*, 2NB_*ac*, 3NB_*abc*, 3NB_*acd*, 4NB and 5NB. Obvious rectifying behavior in 1NB junction and low bias NDR behavior in 4NB junction are shown in the inset.

Figure 2 Transmission spectra under zero bias for models 1NB, 2NB_*ab*, 2NB_*ac*, 3NB_*abc*, 3NB_*acd*, 4NB and 5NB. The energy origin is set to be the Fermi level E_F.

Figure 4 Calculated rectification ratio as a function of the applied bias for models 1NB, 2NB_*ab*, 2NB_*ac*, 3NB_*abc*, 3NB_*acd*, 4NB and 5NB. The inset shows the rectification ratio curves of 3NB_*abc* and 3NB_*acd* junctions.

reduced dramatically when more than one N/B atoms are doped. Interestly, the rectifying direction is even reversed with the change of doping positions. For example, the rectifying direction of 3NB_*abc* junction is opposite to that of 3NB_*acd* junction, as shown in the inset of Figure 4.

The current through 4NB junction is enhanced significantly compared with those through other junctions. In particular, obvious NDR is observed in 4NB junction (which can be seen more clearly from the inset in Figure 3). It can be seen that the current through 4NB junction increases quickly and almost linearly with the increase of applied bias. However, as the bias exceeds 0.4 V (−0.25 V), the current decreases obviously. NDR is a very useful property due to its wide applications such as high-frequency oscillators [18], analog-to-digital converters [19], and logic [20]. Though NDR behavior has been found in a variety of molecular devices, it can typically only be observed at a relatively high bias [21–24]. Thus, the result can be used to develop NDR-based devices for operation at much lower bias to reduce power consumption.

Since the current is the integral of transmission spectra within the bias window (BW), in order to understand the observed rectifying and NDR behaviors, we calculated the transmission spectra under biases 0, ±0.6 V for 1NB junction, 0, −0.25 (peak) and −0.5 (valley) V for 4NB junction, respectively, as shown in Figure 5. For 1NB junction, there are two transmission peaks around E_F in the zero-bias case. Both the peaks shift downward with the increase of applied forward-bias, and the integral area in the BW becomes larger and larger, making a significant increase of $I_{forward}$. On the other hand, the peak below E_F shifts downward while the one above E_F shifts upward with the increase of applied backward-bias. As a result, there is no any transmission peak in the BW, and the electron can only transport through non-resonant tunneling, causing a dramatic suppression of $I_{backward}$. For 4NB junction, there is a broad and strong transmission peak right lies in E_F in the zero-bias case. When −0.25 V bias is applied, the change of this transmis-

sion peak is very little and most part of the peak moves into the BW, resulting in an initial increase in current. However, when −0.5 V bias is applied, this peak shifts downward obviously, and its height reduces simultaneously. The overall reduction in peak height suppresses any gain resulting from a wider BW, leading to a net drop in current. Thus, the NDR appears when bias exceeds −0.25 V.

To understand the origin of those transmission peaks and the reason of their shifts with bias, we projected the density of states (PDOS) onto the left (solid line) and right (dashed line) electrode under biases 0, ±0.6 V for 1NB junction, 0, −0.25 and −0.5 V for 4NB junction, respectively, as shown in Figure 6. It is well known that there is good correspondence between the peaks in the transmission spectrum and those in the PDOS [25]. For 1NB junction, there are three PDOS peaks at −0.26, 0.19, and 0.44 eV in the left and right electrode in the zero-bias case, respectively. The overlap between these two sets of PDOS peaks gives rise to three transmission peaks in the zero-bias transmission spectrum (the middle panel of Figure 5(a)). With the increase of forward-bias, all PDOS peaks shift toward lower energies, which lead to the transmission peaks shifts downward (the top panel of Figure 5(a)). On the contrary, with the increase of backward-bias, PDOS peaks coming from the left electrode shift toward lower energies and the PDOS peak below E_F from the right electrode also shifts downward while the peaks above E_F shift upward. As a result, the transmission peaks are beyond the range of BW (the bottom panel of Figure 5(a)) and have no contribution to the current integral. For 4NB junction, there is large overlap around E_F between two sets of PDOS peaks coming from two electrodes in the zero-bias case. With the increase of backward-bias, the PDOS peaks coming from the left electrode shift toward lower energies while those from the right electrode shift toward higher energies. When −0.25 V bias is applied, the shift of PDOS peaks is very weak, and the overlap around E_F between two sets of PDOS peaks is still very large. Consequently, there is still a strong and broad transmission peak
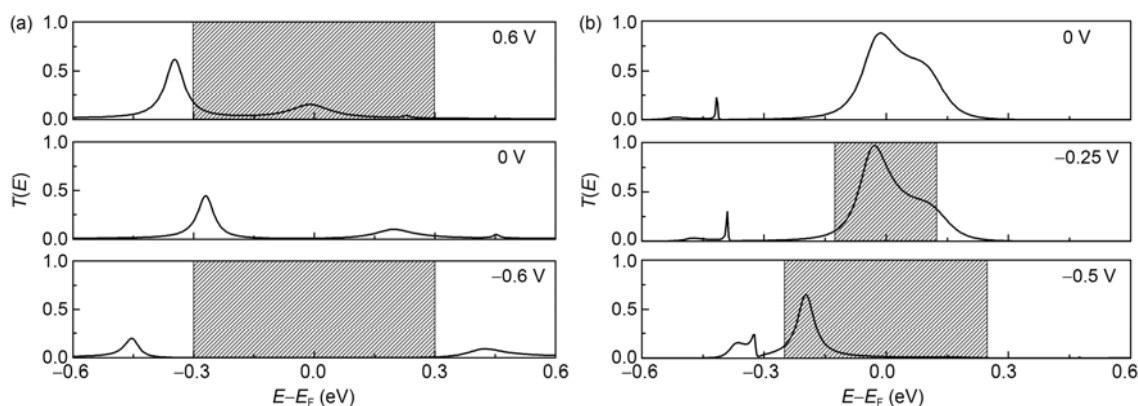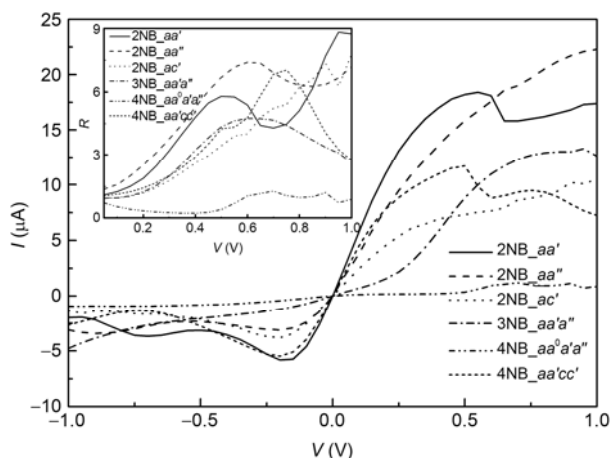

Figure 5   (a) The bias dependence of the transmission spectra under 0.6, 0, and −0.6 V for 1NB junction; (b) the bias dependence of the transmission spectra under 0, −0.25, and −0.5 V for 4NB junction. The shaded region indicates the bias window.
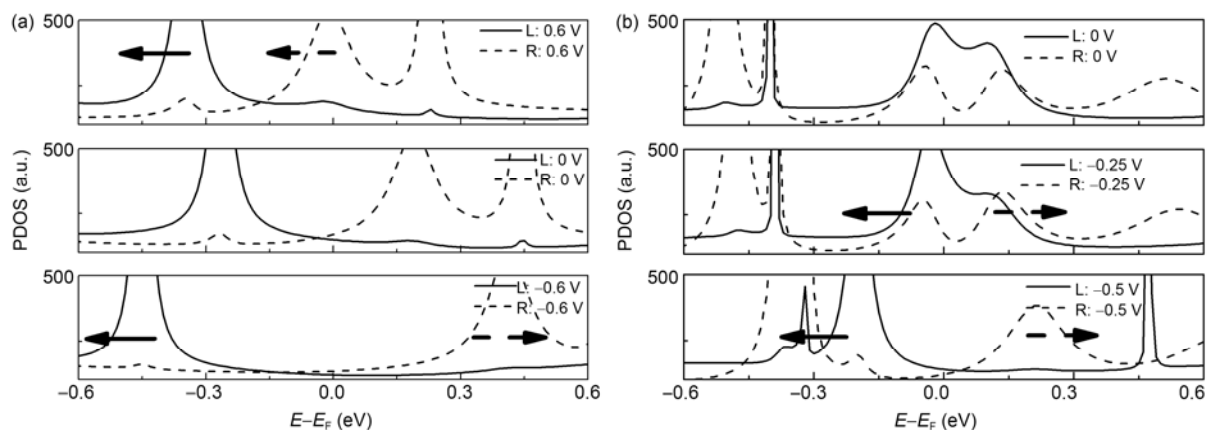
Figure 6 (a) The bias dependence of the PDOS spectra of the left (solid line) and right (dashed line) electrodes under 0.6, 0, and −0.6 V for 1NB junction; (b) the bias dependence of the PDOS spectra of the left (solid line) and right (dashed line) electrodes under 0, −0.25, and −0.5 V for 4NB junction. The characters L and R represent the left and right electrode, respectively. The arrows indicate the shift directions of PDOS with the increase of bias.

within the BW (the middle panel of Figure 5(b)). The shift of PDOS peaks becomes significant with the increase of bias and the overlap around E_F becomes weaker and weaker. As a result, the transmission peak shifts downward and its height decreases simultaneously (the bottom panel of Figure 5(b)).

At last, we explore the effect of doping in different layers on the transport by constructing six models: 2NB_*aa'*, 2NB_*aa''*, 2NB_*ac'*, 3NB_*aa'a''*, 4NB_*aa^{0}a'a''* and 4NB_*aa'cc'*, where a^0, a' (c') and a'' means possible doping positions in the first, third and fourth layers, respectively. The calculated *I-V* and rectification ratio curves are plotted in Figure 7. As we can see, different layers doping can also affect the transport, for example, low-bias NDR (−0.2 V) only appears in 2NB_*aa'*, 2NB_*aa''*, 2NB_*ac'* and 4NB_*aa'cc'*. However, the rectification ratio is still reduced dramatically comparing with the one N/B atoms doping case.

In conclusion, we have investigated the electronic transport properties of capped-SWCNT molecular junctions with multiple N and B dopants by applying NEGF+DFT. The results show that the numbers of N and B atoms and doping positions significantly affect the electronic transport properties of the capped-SWCNT junctions. Best rectifying behavior is obtained in the case with one N and one B dopants, which is deteriorated strongly with the increasing dopants. The rectifying direction is even reversed with the change of doping positions. Moreover, obvious low bias NDR behavior is observed in some doping cases. We believe that the present findings could be helpful for the application of the SWCNTs in the field of high performance rectifying and low bias NDR devices.

Figure 7 *I-V* curves for models 2NB_*aa'*, 2NB_*aa''*, 2NB_*ac'*, 3NB_*aa'a''*, 4NB_*aa^{0}a'a''* and 4NB_*aa'cc'*. The inset shows the corresponding rectification ratio curves.

1   Iijima S. Nature, 1991, 354: 56–58
2   Zhang Z Y, Liang X L, Wang S, et al. Nano Lett, 2007, 7: 3603–3607
3   Zhao P, Wang P J, Zhang Z, et al. Phys Lett A, 2010, 374: 1167–1171
4   Zhao P, Wang P J, Zhang Z, et al. Solid State Commun, 2009, 149: 928–931
5   Khazaei M, Lee S U, Pichierri F, et al. J Phys Chem C, 2007, 111: 12175–12180
6   Shin K, Jeon H, Park C E, et al. Org Electron, 2010, 11: 1403–1407
7   Zhou C W, Kong J, Yenilmez E, et al. Science, 2000, 290: 1552–1555
8   Bachtold A, Hadley P, Nakanishi T, et al. Science, 2001, 294: 1317–1320
9   Stephan O, Ajayan P M, Colliex C, et al. Science, 1994, 266: 1683–1685
10 Terrones M, Benito A M, Manteca-Diego C, et al. Chem Phys Lett, 1996, 257: 576–582
11 Yu J, Ahn J, Yoon S F, et al. Appl Phys Lett, 2000, 77: 1949–1951
12 Han W, Bando Y, Kurashima K, et al. Chem Phys Lett, 1999, 299: 368–373

13 Zhao P, Liu D S. Chin Sci Bull, 2010, 55: 4104–4107
14 Zhao P, Liu D S, Zhang Y, et al. Chin Phys Lett, 2011, 28: 047301
15 Soler J M, Artacho E, Gale J D, et al. J Phys: Condens Matter, 2002, 14: 2745–2779
16 Taylor J, Guo H, Wang J. Phys Rev B, 2001, 63: 245407
17 Brandbyge M, Mozos J L, Ordejón P, et al. Phys Rev B, 2002, 65: 165401
18 Brown E R, Söderström J R, Parker C D, et al. Appl Phys Lett, 1991, 58: 2291–2293
19 Broekaert T P E, Brar B, Van der Wagt J P A, et al. IEEE J Solid State Circuits, 1998, 33: 1342–1349
20 Mathews R H, Sage J P, Sollner T C L G, et al. Proc IEEE, 1999, 87: 596–605
21 Chen J, Reed M A, Rawlett A M, et al. Science, 1999, 286: 1550–1552
22 Long M Q, Chen K Q, Wang L L, et al. Appl Phys Lett, 2008, 92: 243303
23 An Y P, Yang C L, Wang M S, et al. J Phys Chem C, 2009, 113: 15756–15760
24 Zhao P, Fang C F, Xia C J, et al. Appl Phys Lett, 2008, 93: 013113
25 Shi X Q, Dai Z X, Zheng X H, et al. J Phys Chem B, 2006, 110: 16902–16907